

Fully Differentiable and Interpretable Model for VIO with 4 Trainable Parameters

Zexi Chen[†], Haozhe Du[†], Yiyi Liao, Yue Wang, Rong Xiong

Abstract—Monocular visual-inertial odometry (VIO) is a critical problem in robotics and autonomous driving. Traditional methods solve this problem based on filtering or optimization. While being fully interpretable, they rely on manual interference and empirical parameter tuning. On the other hand, learning-based approaches allow for end-to-end training but require a large number of training data to learn millions of parameters. However, the non-interpretable and heavy models hinder the generalization ability. In this paper, we propose a fully differentiable, interpretable, and lightweight monocular VIO model that contains only 4 trainable parameters. Specifically, we first adopt Unscented Kalman Filter as a differentiable layer to predict the pitch and roll, where the covariance matrices of noise are learned to filter out the noise of the IMU raw data. Second, the refined pitch and roll are adopted to retrieve a gravity-aligned BEV image of each frame using differentiable camera projection. Finally, a differentiable pose estimator is utilized to estimate the remaining 4 DoF poses between the BEV frames. Our method allows for learning the covariance matrices end-to-end supervised by the pose estimation loss, demonstrating superior performance to empirical baselines. Experimental results on synthetic and real-world datasets demonstrate that our simple approach is competitive with state-of-the-art methods and generalizes well on unseen scenes.

I. INTRODUCTION

Visual-inertial odometry (VIO) is a fundamental component of the visual-inertial simultaneous localization and mapping system with many applications in robotics and autonomous driving. As a cheap and efficient solution, monocular VIO has attracted growing interest recently. However, monocular VIO is a challenging task considering the limited sensory information.

Traditional monocular VIO approaches have demonstrated promising results based on classical feature detection and feature matching [20, 10, 22, 3], see Fig. 1 (top). These methods are interpretable and generalize well, but require manual interference and empirical parameter tuning. Moreover, these methods only leverage sparse features, resulting in the degraded performance in textureless regions [9].

More recently, learning-based approaches address these limitations by learning the ego-motion in an end-to-end fashion from the raw, dense monocular images, as illustrated in Fig. 1 (middle). However, they lack interpretability and thus pose a new challenge to generalization. While many works improve the interpretability by predicting an intermediate

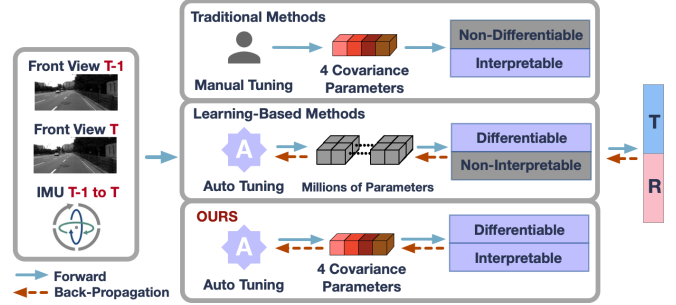


Fig. 1: Comparison of VIO methods. **Top**: the standard visual-inertial odometry framework that requires manual tuning parameters, **middle**: most learning based VIO approaches learn depth or optical flow prediction before a pose regression, and are loaded with tons of heavy parameters for training, and **bottom**: our differential interpretable model based learning approach that solve the problem in an end to end manner, with only 4 trainable parameters.

optical flow [19, 18, 5, 2] or depth map [25, 31, 28, 15], the following pose regression network remains uninterpretable. Furthermore, existing learning-based approaches rely on a large number of training images to learn millions of parameters while the ego-motion has essentially 6 DoF only. We thus ask the following question: *Is it possible to obtain a fully interpretable model with a minimal set of parameters being learned end-to-end?*

In this paper, we aim to combine the advantages of the traditional methods with those of the learning-based approaches. As illustrated in Fig. 1 (bottom), our key idea is to design a fully differentiable, interpretable model that allows for replacing empirical parameter tuning with learning from the data. Additionally, our method exploits dense appearance information instead of sparse features. As it is difficult to differentiate the 6 DoF pose estimation that involves robust and non-linear optimization, we focus on the 4 DoF pose estimation conditioned on the estimated pitch and roll angles. This approximation usually works in driving scenarios, e.g., urban roads and highways, and has gained traction recently [21].

More formally, we consider the monocular VIO as a function that outputs a relative pose taking as input i) two consecutive frames, and ii) IMU data. First, we utilize a Differentiable Unscented Kalman Filter (DUKF) to filter out noise from the IMU raw measurements and retrieve pitch and roll. As the covariance matrices of noise in both the motion model and the measurement model are not known precisely in practice, classical UKF relies on empirical parameter

[†]: Both authors contribute equally.

All authors are with the State Key Laboratory of Industrial Control Technology and Institute of Cyber-Systems and Control, Zhejiang University, Zhejiang, P.R.China. Yue Wang is the corresponding author wangyue@iipc.zju.edu.cn.

tuning given a specific scene. In contrast, we exploit the fact that UKF is differentiable and optimize the covariance matrices in an end-to-end manner leveraging the training data. This requires the estimator of the remaining 4 DoF pose to be differentiable as well. Therefore, in the second step, we estimate the remaining 4 DoF poses by converting monocular images to bird-eye view conditioned on the denoised pitch and roll [21]. The bird-eye view representation allows us to obtain a global optimal solution using Differentiable Phase Correlation (DPC) [4] in a single forward pass. Note that DPC leverages dense appearance information and does not introduce any trainable parameters. More importantly, it allows for back-propagating the gradient to the DUKF module to update the covariance matrices. The combination of DUKF and DPC provides us a fully differentiable, interpretable, and lightweight model for VIO, named BEVO, with 4 parameters of the covariance matrices as the *only* trainable parameters in total. We summarize our contributions as follows:

- We present a fully differentiable, interpretable, and lightweight monocular VIO framework that combines the advantages of both traditional and learning-based approaches.
- We propose to use the Unscented Kalman Filter as a differentiable layer and leverage the Differentiable Phase Correlation on BEV images for pose estimation. This novel combination allows for learning the covariance matrices from data in an end-to-end manner.
- Extensive experiments on KITTI, CARLA, and AeroGround demonstrate that, surprisingly, our simple approach shows competitive results compared to the state-of-the-art.

We will make our code publicly available [here](#).

II. RELATED WORKS

In this section, we will introduce the related works of VIO, mainly divided into two parts, traditional methods and learning-based methods.

A. Traditional Methods

Visual-inertial odometry aims to fuse data from the camera and inertial measurement unit to estimate the ego-motion. Traditional VIO methods are mainly based on filtering and optimization. Mourikis et al. [17] propose a Multi-State Constraint Kalman Filter (MSCKF) method that utilizes the EKF to estimate poses. Moreover, Li et al. [12] improve the MSCKF approach by ensuring the correct observability properties and performing online estimation of calibration parameters. Sun et al. [23] present a stereo version MSCKF which is robust and efficient. OKVIS [11] optimize through keyframe while VINS-Mono [20] is a state estimator based on nonlinear optimization, which contains a tightly coupled visual-inertial odometry and performs global pose graph optimization. These robust methods can generalize well but require empirical parameter tuning which is labor intensive.

B. Learning-based Methods

VINet [6] is the first end-to-end learning-based method for visual-inertial odometry which eliminates the need for manual synchronization and calibration. DeepVO [26] uses Recurrent Convolutional Neural Networks to learn feature representation in visual odometry problems. Wang et al. [27] present TartanVO, which can generalize to multiple datasets and real-world scenarios. DeepVIO [9] merges 2D optical flow features and IMU data to provide absolute trajectory estimation, during which the depth and dense point cloud are estimated. More recent works, e.g., SelfVIO [1], CodeVIO [34], UnDeepVO [13], Li et al. [14], also take advantage of depth estimation to achieve high pose estimation accuracy. However, all methods above train a large network with millions of parameters, resulting in heavy models and are merely interpretable with weak generalization ability. Therefore, we set to solve this problem by introducing a fully interpretable model with only 4 trainable parameters.

III. FULLY DIFFERENTIABLE AND INTERPRETABLE MODEL FOR VIO

We aim to estimate the odometry with the input of one monocular camera and IMU data by a differentiable and interpretable model. Following the pipeline in Fig. 2, we employ a trainable UKF to integrate IMU data for pitch and roll estimation. Then the denoised pitch and roll, together with the corresponding front image are fed into the second differentiable module, for differentiable pose estimation of the remaining 4 DoF pose. To this goal, we transform the image to the BEV images conditioned on the denoised pitch and roll. Following the BEV projection, the $\text{SIM}(2)$ pose of two consecutive BEV images is estimated by the DPC. Note that the UKF is a continuous forward function and is differentiable in essence. In this work, we emphasize its backward path by referring to it as DUKF, to distinguish it from the traditional UKF utilization which focuses only on the forward path. As a result, the only trainable parameters are the 4 numbers that make up the covariance matrices of motion and measurement in the DUKF and are trained end-to-end with the pose loss altogether.

A. Differentiable Unscented Kalman Filter

For the DUKF, there are two basic models in the pipeline, namely, the motion model and measurement model.

Motion Model: Given a consecutive series of pitch rate and roll rate from the IMU raw data from time $t-1$ to t , and the filtered pitch and roll in time $t-1$, we have the state in time $t-1$ as:

$$x_{t-1} = [\alpha_{t-1}, \beta_{t-1}]^T, \quad (1)$$

where α , and β are the pitch and roll angle respectively. Following the sampling theory of UKF [24], the sampled state in $t-1$ becomes:

$$X_{t-1} = \Gamma(x_{t-1}), \quad (2)$$

where Γ is the sampling rule. Given the motion model G , we have the initial guess of pitch and roll in time t as:

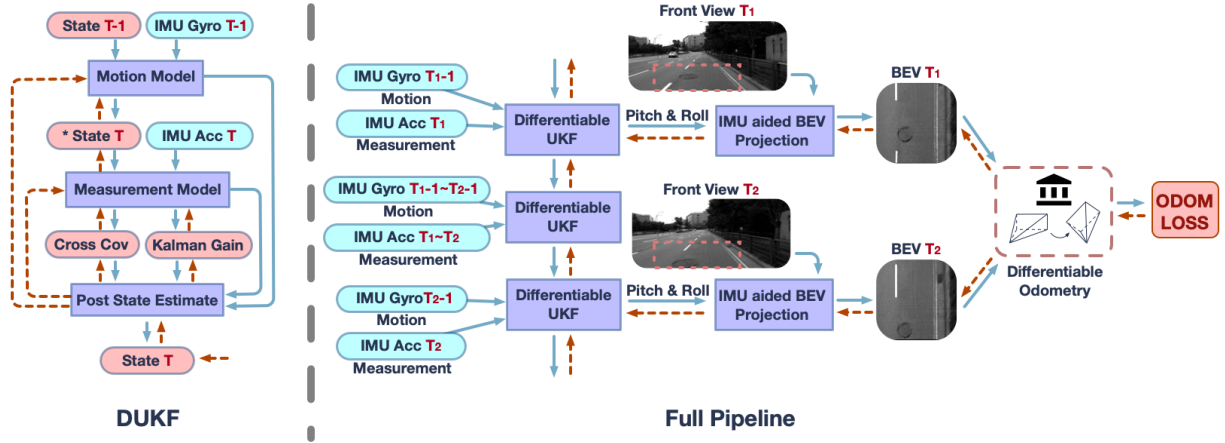


Fig. 2: The overall pipeline of the proposed BEVO. As a demonstration, the frequency of the front image is 10Hz while the frequency of IMU is 100Hz. For each frame of IMU, the pitch rate, roll rate, and 3D acceleration are fed into the differentiable UKF to learn noise filtering (elaborated in the left part of the figure). However, due to the frequency difference, only frames with front images have back-propagated gradients (red dashed lines) for the DUKF training.

$$\bar{X}_t^* = G(X_{t-1}) = [\alpha_{t-1} + \omega_{\alpha_{t-1}}, \beta_{t-1} + \omega_{\beta_{t-1}}]^T \quad (3)$$

$$\bar{\mu}_t = \sum w_m \bar{X}_t^* \quad (4)$$

$$\bar{\sigma}_t = \sum w_c (\bar{X}_t^* - \bar{\mu}_t)(\bar{X}_t^* - \bar{\mu}_t)^T + \mathbf{O}_t, \quad (5)$$

where ω_α , and ω_β are the pitch and roll rate from the gyroscope, and $\bar{\mu}_t$ and $\bar{\sigma}_t$ are the mean and variance of the initial guess of \bar{X}_t^* , respectively. Note that w_m and w_c are the weights for each sampled state in \bar{X}_t^* based on the theory in [24], and \mathbf{O}_t is the covariance matrix for the noise of the motion model to be trained. Since \mathbf{O}_t is a 2×2 diagonal matrix, we parameterize it with the two parameters on the diagonal.

Measurement Model: After updating the covariance matrix \mathbf{O}_t , we retrieve a new sampled state \bar{X}_t in time t :

$$\bar{x}_t \sim N(\bar{\mu}_t, \bar{\sigma}_t) \triangleq [\bar{\alpha}_t, \bar{\beta}_t]^T \quad (6)$$

$$\bar{X}_t = \Gamma(\bar{x}_t), \quad (7)$$

where x_t satisfies the normal distribution. Given the measurement model H , the initial guess of measurement is

$$\bar{Z}_t = H(\bar{X}_t) = [\bar{\alpha}_t, \bar{\beta}_t]^T \quad (8)$$

$$\bar{M}_t = \sum w_m \bar{Z}_t \quad (9)$$

$$\bar{\Sigma}_t = \sum w_c (\bar{Z}_t - \bar{M}_t)(\bar{Z}_t - \bar{M}_t)^T + \mathbf{Q}_t, \quad (10)$$

where \bar{M}_t and $\bar{\Sigma}_t$ are the mean and variance of \bar{X}_t respectively, and \mathbf{Q}_t is the covariance matrix for the noise of the measurement model to be trained and is parametrized following the same rule as \mathbf{O}_t .

Now, considering a real-world measurement is obtained:

$$\hat{\alpha}_t = \arctan(acc_t^x / acc_t^z) \quad (11)$$

$$\hat{\beta}_t = -\arctan(acc_t^y / \sqrt{acc_t^x^2 + acc_t^z^2}) \quad (12)$$

$$\mathbf{Z}_t = [\hat{\alpha}_t, \hat{\beta}_t]^T, \quad (13)$$

where $\hat{\alpha}_t$ and $\hat{\beta}_t$ are the measurement of pitch and roll in time t with respect to the raw acceleration data in each axes acc_t^x ,

acc_t^y , and acc_t^z . Altogether, the real-world measurement state is formed as \mathbf{Z}_t .

By now, we come to the last stage of the DUKF: update the final state x_t .

$$\bar{\Sigma}_t^{X,Z} = \sum_{i=0}^{2n} w_c^i (\bar{X}_t^i - \bar{\mu}_t)(\bar{Z}_t^i - \bar{M}_t)^T \quad (14)$$

$$\mathbf{K}_t = \bar{\Sigma}_t^{X,Z} \bar{\Sigma}_t^{-1} \quad (15)$$

$$\mu_t = \bar{\mu}_t + \mathbf{K}_t (\mathbf{Z}_t - \bar{M}_t) \quad (16)$$

$$\sigma_t = \bar{\sigma}_t + \mathbf{K}_t \bar{\Sigma}_t \mathbf{K}_t^T \quad (17)$$

$$x_t \sim N(\mu_t, \sigma_t) \triangleq [\alpha_t, \beta_t]^T \quad (18)$$

where $\bar{\Sigma}_t^{X,Z}$, \mathbf{K}_t are the cross-covariance and Kalman Gain respectively, μ_t and σ_t are the mean and variance of x_t which will also guide the sampling in the following time $t + 1$.

B. Differentiable Bird-eye View Projection

To achieve the projection from the front view to the birds-eye view, we first define the transformation matrix from the IMU to the world frame considering its pitch, roll, and elevation:

$$\mathbf{R}_t^{IMU} = \begin{bmatrix} \cos\beta_t & \sin\beta_t & 0 \\ -\cos\alpha_t \sin\beta_t & \cos\alpha_t \cos\beta_t & \sin\alpha_t \\ \sin\alpha_t \sin\beta_t & -\sin\alpha_t \cos\beta_t & \cos\alpha_t \end{bmatrix} \quad (19)$$

$$\mathbf{T}_t^{IMU} = [0 \ 0 \ const_z]^T, \quad (20)$$

the rotation matrix \mathbf{R}_t^{IMU} of the IMU at time t changes constantly with α_t and β_t which are estimated by the DUKF. The translation vector \mathbf{T}_t^{IMU} of the IMU is known and fixed since it is the urban road and highway that we are considering in which the height of the IMU to the ground $const_z$ stays unchanged through the journey [21]. Transformation matrices from camera to the world $[\mathbf{R}_t^{CAM}, \mathbf{T}_t^{CAM}]$ are obtained with extrinsic calibration of $[\mathbf{R}_t^{IMU}, \mathbf{T}_t^{IMU}]$.

Besides the unchanged height, one more assumption can be made for a safe trip: there should be a valuable space in front of the vehicle, forming that the center bottom part of

the front image should represent a plane ground, shown as the red dashed box in Fig. 2.

With the assumption above, we consider pixels within the red dashed box as a set of points in the 3D space, and map them from the camera plane to the ground plane.

To begin with, we generate a set of even points P_g on the ground plane that stand for the location that the BEV should be projected:

$$P_g \triangleq \{X', Y', Z'\}^T, \quad (21)$$

where $X', Y',$ and Z' are the coordinates of points. P_g is then transformed to the camera coordinate with:

$$P_c^t = R_t^{CAM^T} (P_g - T_t^{CAM}) \triangleq \{X_t'', Y_t'', Z_t''\}^T, \quad (22)$$

and P_c^t is projected to the camera plane with the focal lengths f_x, f_y and principal point (c_x, c_y) :

$$Z_t'' \begin{bmatrix} u_t' \\ v_t' \\ 1 \end{bmatrix} = \begin{bmatrix} f_x & 0 & c_x \\ 0 & f_y & c_y \\ 0 & 0 & 1 \end{bmatrix} \begin{bmatrix} X_t'' \\ Y_t'' \\ Z_t'' \end{bmatrix}, \quad (23)$$

where (u_t', v_t') are the indexes on the front camera image of each corresponding point in P_g in time t . Therefore, by remapping the original pixels (u, v) to (u_t', v_t') , we can further retrieve the BEV projection I_t^{bev} out of the red dashed box I_t^f in Fig. 2.

$$I_t^{bev} = F_{(u,v)}^{(u_t', v_t')}(I_t^f), \quad (24)$$

$F_{(u,v)}^{(u_t', v_t')}(\cdot)$ is the remapping of \cdot from (u, v) to (u_t', v_t') . Since it is parameterized by the pitch and roll, which is related to the variance of the IMU data, with the help of DUKF, the gradient can be back-propagated to the variance.

C. Differentiable Phase Correlation

Given two images I_{t-1}^{bev} and I_t^{bev} with pose transformations, a variation of the differentiable phase correlation [4] is utilized to estimate the overall relative pose ξ_i between I_{t-1}^{bev} and I_t^{bev} . The rotation and scale is calculated by

$$p(\xi_i^{\theta,s}) = \mathfrak{C}(\mathfrak{L}(\mathfrak{F}(I_t^{bev})), \mathfrak{L}(\mathfrak{F}(I_{t-1}^{bev}))) \quad (25)$$

$$(\theta_t, s_t) = \mathbb{E}(p(\xi_i^{\theta,s})), \quad (26)$$

where $\xi_i^{\theta,s}$ is the rotation and scale part of ξ_i between I_{t-1}^{bev} and I_t^{bev} , \mathfrak{F} is the discrete Fourier Transform, \mathfrak{L} is the log-polar transform, and \mathfrak{C} is the phase correlation solver. Fourier Transformation \mathfrak{F} transforms images into the Fourier frequency domain of which the magnitude has the property of translational insensitivity, therefore the rotation and scale are decoupled with displacements and are represented in the magnitude. Log-polar transformation \mathfrak{L} transforms Cartesian coordinates into log-polar coordinates so that such rotation and scale in the magnitude of Fourier domain are remapped into displacement in the new coordinates, making it solvable with the afterward phase correlation solver. Phase correlation solver \mathfrak{C} outputs a heatmap indicating the displacements of the two log-polar images, which eventually stands for the rotation θ_t and scale s_t of the two input images I_{t-1}^{bev} and I_t^{bev} . To make the solver differentiable, we use expectation $\mathbb{E}(\cdot)$ as the estimation of \cdot .

Then I_t^{bev} is rotated and scaled referring to $\xi_t^{\theta,s}$ with the result of \bar{I}_t^{bev} :

$$\bar{I}_t^{bev} = \begin{bmatrix} s_t R_{\theta_t} & 0 \\ 0 & 1 \end{bmatrix} I_t^{bev}. \quad (27)$$

In the same manner, translations ξ_t^t between \bar{I}_t^{bev} and I_{t-1}^{bev} is calculated

$$p(\xi_t^t) = \mathfrak{C}(\bar{I}_t^{bev}, I_{t-1}^{bev}) \quad (28)$$

$$\mathbf{t}_t = \mathbb{E}(p(\xi_t^t)). \quad (29)$$

With the relative rotation θ_t , scale s_t , and translation \mathbf{t}_t between I_{t-1}^{bev} and I_t^{bev} , and by consulting with the fixed *Distance per Pixel* (DDP), we finally arrive at the *SIM(2)* pose between frame $t-1$ and t of vehicle:

$$S_t = [\theta_t, s_t, DDP \cdot \mathbf{t}_t]. \quad (30)$$

Note that the gradient in the part can be back-propagated all the way back to the variance of the IMU data since the phase correlation is differentiable.

D. Loss Design, Back-Propagation, and Training

With the elaboration above, we define a one-step VIO as a function:

$$T = \mathcal{VIO}_{O,Q}(I_{t-1}, I_t, \omega, a) \quad (31)$$

where $\mathcal{VIO}_{O,Q}$ is fully differentiable and interpretable with 4 trainable parameters in O_t and Q_t . I , ω , and a are the front images, gyroscope data, and accelerometer data. Since the network is fully differentiable, it is trained end to end and supervised only with the ground truth of the odometry between frames. Such supervision is applied to optimize the covariance matrices of noise in both the motion model and the measurement model of DUKF.

Elaborately, we wish to supervise the distribution of the poses $\xi_t^{\theta,s}$ and ξ_t^t and therefore, we calculate the Kullback-Leibler Divergence loss KLD between $\{p(\xi_t^{\theta,s}), p(\xi_t^t)\}$ and the ground truth:

$$\mathcal{L} = KLD(p(\xi_t^{\theta,s}), \mathbf{1}_{\theta_{GT}}) + KLD(p(\xi_t^t), \mathbf{1}_{\mathbf{t}_{GT}}) \quad (32)$$

where $\mathbf{1}_{\theta_{GT}}$ and $\mathbf{1}_{\mathbf{t}_{GT}}$ are the Gaussian Blurred one-peak distributions centered at the ground truth θ_{GT} and \mathbf{t}_{GT} respectively.

Training Details: all trainings are conducted on a GPU server with two NVIDIA RTX 3090 as GPUS and Intel i9 9900k as the CPU. For the optimizer, we choose the ADAM. We only supervise the model with 4 DoF ground truth (GT) data of the same frequency as the images, i.e. the high frequency GT of the IMU is not needed.

Plug into Map-Based Localization System: in addition to the odometry, we also explore the possibility of integrating BEVO with fully differentiable localization to achieve a drift-free system. However, this is not the focus of our work and therefore we will not elaborate upon it, but show result as demonstration of the application.

IV. EXPERIMENTAL SETUP

We conduct two main experiments: i) odometry estimation on the KITTI [8] odometry dataset on which the experiments on ablation study, testing, generalization are conducted, and ii) heterogeneous localization on CARLA [7] and the AeroGround Dastat [32].

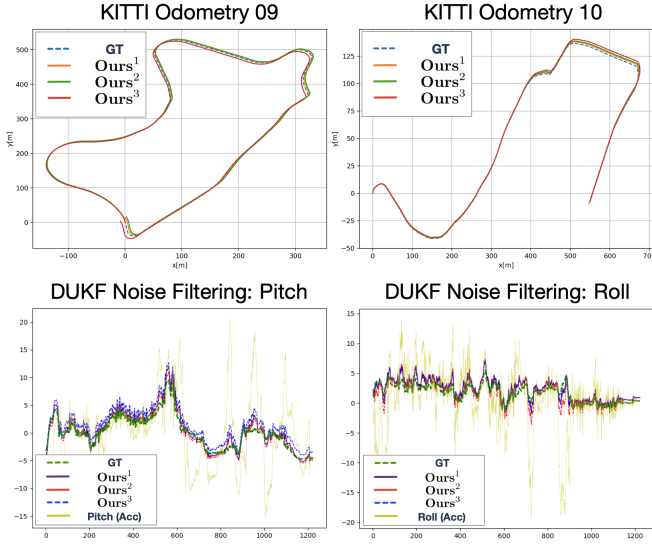


Fig. 3: **Top:** The qualitative results of the evaluation on KITTI sequence 09, and 10. **Bottom:** Noise filtering of the pitch and roll angle through sequence 10. It indicates that even though pitch and roll are not directly supervised, the low-frequency image-level supervision in 4 DoF *only* still allows the model to obtain good results in pitch and roll.

A. Dataset and Corresponding Experiments

KITTI: We evaluate BEVO on the KITTI odometry dataset using sequences 00-08 for training and 09-10 for the test following the same train/validate/test split as [16, 14]. In addition to the widely adopted train/validate split where 20% samples are randomly sampled from the training set for validation, we also train our model in the first three quarters of each sequence of 00-08, and evaluate the performance in the last quarter. This train/validate split is more realistic even though it might present a worse result. Note that sequence 03 cannot be used for training or evaluation in this study since the raw data where we grab the IMU data is missing.

CARLA & AG: We further verify the plausibility of applying the BEVO as a front-end plugin for end-to-end heterogeneous localization following the routine in [29]. Such experiments are conducted in the simulator CARLA and on the real-world AeroGround Dataset.

- **CARLA:** In CARLA, we localize a vehicle on the satellite map in different weathers. We train and utilize BEVO as the odometry and localize the projected BEV (from different weathers) on the heterogeneous satellite map.
- **AeroGround:** The AeroGround (AG) Dataset is collected for multi-robot collaboration. In this dataset, we train and utilize BEVO as the odometry and localize the ground robot with its front camera BEV on the heterogeneous map built by a drone.

B. Evaluation Metrics

We evaluate our trajectories using t_{rel} and r_{rel} from the standard KITTI toolkit as in [14]. In our case, we do not estimate the elevation due to the assumption that the vehicle will not leave the ground. However, we still recorded the initial elevation and keep it constant through the journey for

comparison, which might degrade the performance in t_{rel} to some extent.

C. Baselines

For the odometry experiment, we compare to both traditional method VINS[20] and SOTA depth dependent learning-based methods DEEPVIO[9], LI ET AL. [14], GEONET[30], SELFVIO[1], and depth independent learning-based method TARTANVO[27]. For the localization experiments, we compare the performance with VINS-MONO [20].

V. EXPERIMENTAL RESULTS

A. Ablation Study

We conduct several ablation studies on KITTI to validate the effectiveness of the proposed DUKF as well as the learned covariance matrices.

Several experiments conducted in KITTI are designed for the ablation study to reassure the important role a DUKF plays in the BEVO as well as the role trainable covariance matrices play in DUKF. First, we replace the learned covariance matrix O_t by one that is empirically set in [24]. The quantitative result in Table. II shows that the accuracy drops drastically when using a manually tuned matrix, suggesting that the empirical parameter tuning leads to inaccurate pitch and roll estimation, and subsequently deteriorates the BEV generation and odometry estimation. Next, we restore O_t with the learned matrix and replace Q_t with an empirical covariance matrix as [24], and note it as “w/o Q_t ”. The quantitative result also verifies that trainable covariance matrices for noise help to improve the performance of UKF. However, even though the performances are degraded with empirical parameters, they are still competitive due to the dense matching of DPC who seeks global optima.

We further study the importance of DUKF on the BEVO by eliminating the whole DUKF and fed the raw pitch and roll (directly calculated from the accelerometer) to the BEV projection. We note it as “w/o DUKF”. The quantitative result shown in Table. II proves that when the filter is gone, the BEVO will encounter serious tracking failure in bumpy roads. One more ablation study is conducted by replacing the output pitch and roll of DUKF with the ground truth, denoted as “w GT”. The result that BEVO’s performance is comparable with “w GT” indicates that by learning the covariance matrices, the error brought by DUKF is too small to influence the odometry than the error by brought by DPC, showing the effectiveness of the training.

B. Odometry Estimation

We now compare the odometry estimation performance of the proposed BEVO to the state-of-the-art methods in two training settings from section IV-A: i) following train/validate splits in [16][14] (**Ours**¹), and ii) split each sequence by quarters, take the first three quarters of each sequence to train and the last quarter to validate (**Ours**²). In addition to these two settings, we further train BEVO using the first 20% of the training data of each sequence in **Ours**² to evaluate its performance on insufficient data (**Ours**³).

TABLE I: Quantitative results of odometry estimation on KITTI dataset from sequence 00 to 10. **Red** indicates the best performance and **Blue** indicates the second.

Seq	frames	DeepVIO		TartanVO		Li et al.		GeoNet		SelfVIO		VINS		Ours ¹		Ours ²		Ours ³	
		t_{rel}	r_{rel}	t_{rel}	r_{rel}	t_{rel}	r_{rel}	t_{rel}	r_{rel}	t_{rel}	r_{rel}	t_{rel}	r_{rel}	t_{rel}	r_{rel}	t_{rel}	r_{rel}	t_{rel}	r_{rel}
00	4541	11.62	2.45	\	\	14.21	5.93	44.08	14.89	1.24	0.45	18.83	2.49	3.26	1.44	1.55	0.83	2.01	1.02
01	1101	\	\	\	\	21.36	4.62	43.21	8.42	\	\	\	\	5.62	3.95	1.17	1.66	1.76	2.13
02	4661	4.52	1.44	\	\	16.21	2.60	73.59	12.53	0.80	0.25	21.03	2.61	4.56	1.32	1.02	0.88	1.79	1.55
04	271	\	\	\	\	9.08	4.41	17.91	9.95	\	\	\	\	3.79	1.05	2.04	0.92	3.12	1.15
05	2761	2.86	2.32	\	\	24.82	6.33	32.47	13.12	0.89	0.63	21.90	2.72	2.05	1.57	0.72	1.01	1.55	1.80
06	1101	\	\	4.72	2.95	9.77	3.58	40.28	16.68	\	\	\	\	3.86	2.08	1.07	1.56	2.77	1.99
07	1101	2.71	1.66	4.32	3.41	12.85	2.30	37.13	17.20	0.91	0.49	15.39	2.42	3.58	1.47	0.88	1.35	1.15	1.79
08	4701	2.13	1.02	\	\	27.10	7.81	11.45	62.45	1.09	0.36	32.66	3.09	1.94	1.04	0.93	0.92	1.29	1.00
09	1591	1.38	1.12	6.0	3.11	15.21	5.28	13.02	67.06	1.95	1.15	41.47	2.41	1.22	1.05	1.29	1.12	1.32	1.31
10	1201	0.85	1.03	6.89	2.73	25.63	7.69	58.52	23.02	1.81	1.30	20.35	2.73	1.01	1.01	1.14	1.03	1.17	1.30
Ave 00-10		3.73	1.57	5.48	3.05	16.02	4.60	33.78	22.30	1.24	0.67	21.61	2.64	2.80	1.45	1.07	1.02	1.63	1.36
Ave 09-10		1.12	1.08	6.74	2.92	20.42	6.49	35.77	45.04	1.88	1.23	30.91	2.57	1.12	1.03	1.22	1.07	1.24	1.31

TABLE II: Quantitative results of ablation study conducted on KITTI. All of the methods are trained in sequence 00-08 following the train split in [14] and tested in sequence 09-10.

Seq	w/o O_t		w/o Q_t		w/o DUKF		BEVO		w GT	
	t_{rel}	r_{rel}	t_{rel}	r_{rel}	t_{rel}	r_{rel}	t_{rel}	r_{rel}	t_{rel}	r_{rel}
09	4.82	4.73	5.90	5.11	22.05	71.58	1.29	1.12	1.05	1.04
10	5.66	4.87	6.26	5.62	25.64	68.54	1.14	1.03	0.96	1.01

TABLE III: Quantitative results of localization. Note: in CARLA, we localize the vehicle in different weathers against a sunny satellite map, CARLA-S means the vehicle runs in a sunny weather, CARLA-F means the vehicle is in a foggy weather, and CARLA-N means the vehicle runs at night.

Dataset	BEVO		VINS-Mono		BEVO+	
	t_{rel}	r_{rel}	t_{rel}	r_{rel}	t_{rel}	r_{rel}
CARLA-S	1.05	1.82	2.06	2.58	0.21	0.33
CARLA-F	1.11	1.38	2.92	2.14	0.24	0.31
CARLA-N	0.98	1.03	1.82	1.47	0.19	0.28
AG	1.39	1.72	2.55	2.41	0.30	0.46

Fig.3 and Table I show the qualitative and quantitative comparisons, respectively. Table I shows that when trained in the same settings as other baselines, **Ours**² outperforms most of the baselines in validation results in sequence 00 to 08. However, regarding the unseen testing sequences, our **Ours**¹ beats all other baseline in both t_{rel} and r_{rel} except for the t_{rel} of DEEPVIO in sequence 10. This may be explained by the fact that DEEPVIO utilizes stereo cameras instead of monocular camera considered in our method. The result of the testing sequence shows that our method is better at generalization compared to other learning-based methods.

It is worth addressing that with only 4 trainable parameters and without employing any nonlinear optimization such as sliding window, our method is surprisingly comparable with others on sequences 00-08, and is even slightly better in testing on sequences 09 and 10. The result of **Ours**³ suggests that, in contrast to learning-based approaches reliant on a large number of training images, our method is more data-efficient thanks to the lightweight parameters and the fully interpretable model.

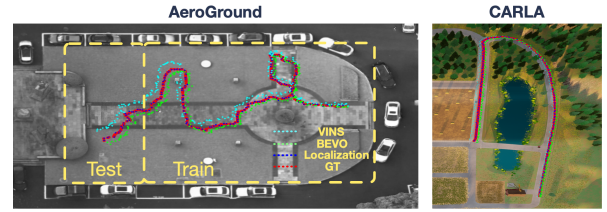


Fig. 4: The demonstration of localizing a front camera's BEV of a ground moving robot in drone's map.

C. Plugin for Heterogeneous Localization

In this part, we show the possibility of enabling an end-to-end localization with BEVO as the odometry following our previous work [29]. Elaborations on the implementation details of the fully differentiable drift-free localization can be found in the supplementary material [33]. By combining BEVO with the heterogeneous localization RALL (denoted as BEVO+), the whole pipeline is fully differentiable, thus allowing for more accurate pose estimation.

We conduct experiments in CARLA and the real-world AG dataset and compare the localization with BEVO itself as well as the VINS-MONO. Results in Fig. 4 and Table II proves that the BEVO is able to achieve good performance even when it acts as a plugin in an end-to-end trainable localization framework. It indicates a promising future for upcoming end-to-end autonomous driving, e.g., auto weeder.

VI. CONCLUSION

We present a fully differentiable, interpretable and lightweight model for monocular VIO, namely, *BEVO*. Our model comprises a UKF to denoise pitch and roll via trainable covariance matrices, a BEV projection, and a differentiable phase correlation to estimate the $\text{SIM}(2)$ pose on the BEV image. The full pipeline is differentiable, allowing us to train the covariance matrices end-to-end and thus avoiding empirical parameter tuning. In various experiments, *BEVO* presents competitive performance in accuracy and generalization. We believe our interpretable, simple approach provides an alternative perspective of traditional methods and should be considered as a baseline for future works on learning-based monocular VIO.

REFERENCES

- [1] Yasin Almalioglu et al. “Selfvio: Self-supervised deep monocular visual-inertial odometry and depth estimation”. In: *arXiv preprint arXiv:1911.09968* (2019).
- [2] Xicheng Ban et al. “Monocular visual odometry based on depth and optical flow using deep learning”. In: *IEEE Transactions on Instrumentation and Measurement* 70 (2020), pp. 1–19.
- [3] Martin Brossard, Silvere Bonnabel, and Axel Barrau. “Unscented Kalman filter on Lie groups for visual inertial odometry”. In: *2018 IEEE/RSJ International Conference on Intelligent Robots and Systems (IROS)*. IEEE. 2018, pp. 649–655.
- [4] Zexi Chen et al. “Deep Phase Correlation for End-to-End Heterogeneous Sensor Measurements Matching”. In: *arXiv preprint arXiv:2008.09474* (2020).
- [5] Cheng Chuanqi et al. “Monocular visual odometry based on optical flow and feature matching”. In: *2017 29th Chinese Control And Decision Conference (CCDC)*. IEEE. 2017, pp. 4554–4558.
- [6] Ronald Clark et al. “Vinet: Visual-inertial odometry as a sequence-to-sequence learning problem”. In: *Proceedings of the AAAI Conference on Artificial Intelligence*. Vol. 31. 1. 2017.
- [7] Alexey Dosovitskiy et al. “CARLA: An open urban driving simulator”. In: *Conference on robot learning*. PMLR. 2017, pp. 1–16.
- [8] Andreas Geiger et al. “Vision meets robotics: The kitti dataset”. In: *The International Journal of Robotics Research* 32.11 (2013), pp. 1231–1237.
- [9] Liming Han et al. “Deepvio: Self-supervised deep learning of monocular visual inertial odometry using 3d geometric constraints”. In: *2019 IEEE/RSJ International Conference on Intelligent Robots and Systems (IROS)*. IEEE. 2019, pp. 6906–6913.
- [10] Yijia He et al. “PI-vio: Tightly-coupled monocular visual-inertial odometry using point and line features”. In: *Sensors* 18.4 (2018), p. 1159.
- [11] Stefan Leutenegger et al. “Keyframe-based visual-inertial odometry using nonlinear optimization”. In: *The International Journal of Robotics Research* 34.3 (2015), pp. 314–334.
- [12] Mingyang Li and Anastasios I Mourikis. “High-precision, consistent EKF-based visual-inertial odometry”. In: *The International Journal of Robotics Research* 32.6 (2013), pp. 690–711.
- [13] Ruihao Li et al. “Undeepvo: Monocular visual odometry through unsupervised deep learning”. In: *2018 IEEE international conference on robotics and automation (ICRA)*. IEEE. 2018, pp. 7286–7291.
- [14] Shunkai Li et al. “Self-supervised deep visual odometry with online adaptation”. In: *Proceedings of the IEEE/CVF Conference on Computer Vision and Pattern Recognition*. 2020, pp. 6339–6348.
- [15] Xiangyu Li et al. “Dvonet: unsupervised monocular depth estimation and visual odometry”. In: *2019 IEEE Visual Communications and Image Processing (VCIP)*. IEEE. 2019, pp. 1–4.
- [16] Reza Mahjourian, Martin Wicke, and Anelia Angelova. “Unsupervised learning of depth and ego-motion from monocular video using 3d geometric constraints”. In: *Proceedings of the IEEE Conference on Computer Vision and Pattern Recognition*. 2018, pp. 5667–5675.
- [17] Anastasios I Mourikis and Stergios I Roumeliotis. “A multi-state constraint Kalman filter for vision-aided inertial navigation”. In: *Proceedings 2007 IEEE International Conference on Robotics and Automation*. IEEE. 2007, pp. 3565–3572.
- [18] Peter Muller and Andreas Savakis. “Flowdometry: An optical flow and deep learning based approach to visual odometry”. In: *2017 IEEE Winter Conference on Applications of Computer Vision (WACV)*. IEEE. 2017, pp. 624–631.
- [19] Tejas Pandey et al. “Leveraging deep learning for visual odometry using optical flow”. In: *Sensors* 21.4 (2021), p. 1313.
- [20] Tong Qin, Peiliang Li, and Shaojie Shen. “Vins-mono: A robust and versatile monocular visual-inertial state estimator”. In: *IEEE Transactions on Robotics* 34.4 (2018), pp. 1004–1020.
- [21] Tong Qin et al. “Avp-slam: Semantic visual mapping and localization for autonomous vehicles in the parking lot”. In: *2020 IEEE/RSJ International Conference on Intelligent Robots and Systems (IROS)*. IEEE. 2020, pp. 5939–5945.
- [22] Ethan Rublee et al. “ORB: An efficient alternative to SIFT or SURF”. In: *2011 International conference on computer vision*. Ieee. 2011, pp. 2564–2571.
- [23] Ke Sun et al. “Robust stereo visual inertial odometry for fast autonomous flight”. In: *IEEE Robotics and Automation Letters* 3.2 (2018), pp. 965–972.
- [24] Eric A Wan, Rudolph Van Der Merwe, and Simon Haykin. “The unscented Kalman filter”. In: *Kalman filtering and neural networks* 5.2007 (2001), pp. 221–280.
- [25] Rui Wang, Stephen M Pizer, and Jan-Michael Frahm. “Recurrent neural network for (un-) supervised learning of monocular video visual odometry and depth”. In: *Proceedings of the IEEE/CVF Conference on Computer Vision and Pattern Recognition*. 2019, pp. 5555–5564.
- [26] Sen Wang et al. “Deepvo: Towards end-to-end visual odometry with deep recurrent convolutional neural networks”. In: *2017 IEEE International Conference on Robotics and Automation (ICRA)*. IEEE. 2017, pp. 2043–2050.
- [27] Wenshan Wang, Yaoyu Hu, and Sebastian Scherer. “TartanVO: A Generalizable Learning-based VO”. In: *arXiv preprint arXiv:2011.00359* (2020).
- [28] Mingkang Xiong et al. “Self-supervised Monocular Depth and Visual Odometry Learning with Scale-

- consistent Geometric Constraints.” In: *IJCAI*. 2020, pp. 963–969.
- [29] Huan Yin et al. “Rall: end-to-end radar localization on lidar map using differentiable measurement model”. In: *IEEE Transactions on Intelligent Transportation Systems* (2021).
 - [30] Zhichao Yin and Jianping Shi. “Geonet: Unsupervised learning of dense depth, optical flow and camera pose”. In: *Proceedings of the IEEE conference on computer vision and pattern recognition*. 2018, pp. 1983–1992.
 - [31] Huangying Zhan et al. “Unsupervised learning of monocular depth estimation and visual odometry with deep feature reconstruction”. In: *Proceedings of the IEEE conference on computer vision and pattern recognition*. 2018, pp. 340–349.
 - [32] ZJU-Robotics-Lab. *AeroGround Dataset*. 2020. URL: <https://github.com/ZJU-Robotics-Lab/OpenDataSet>.
 - [33] ZJU-Robotics-Lab. *Supplementary Material*. 2020. URL: https://github.com/jessychen1016/BEVO_pytorch.
 - [34] Xingxing Zuo et al. “CodeVIO: Visual-Inertial Odometry with Learned Optimizable Dense Depth”. In: *arXiv preprint arXiv:2012.10133* (2020).